Globally exponentially stable wind estimation for small fixed-wing UAVs using standard sensors

Bård N. Stovner* and Tor A. Johansen†
Center for Autonomous Marine Operations and Systems (NTNU-AMOS), Department of Engineering Cybernetics, Norwegian University of Science and Technology, Trondheim, Norway

This paper considers the estimation of the steady wind component around small fixed-wing unmanned aerial vehicles using measurements from a Pitot-static tube and velocity over ground information. A three-stage filter is proposed, which yields globally exponentially stable estimation of the wind velocity and a correction factor on the dynamic pressure measurements from the Pitot-static tube. The suggested filter is compared with an extended Kalman filter and shown to yield identical steady state performance in both simulations and experiments. Additionally, the improved stability with respect to the extended Kalman filter is demonstrated with a choice of suboptimal tuning, for which the extended Kalman filter failed to converge whereas the suggested filter did not.

I. INTRODUCTION

Wind influences aircraft motion, and having an estimate of the wind velocity is therefore useful for control and safety monitoring. Knowledge about angle of attack (AOA), sideslip angle (SSA), and airspeed is crucial for safe and efficient flight of fixed-wing aircrafts. It is common for large airplanes to use a multi-hole Pitot tube or a combination of vanes and a single-hole Pitot tube to measure them directly. For smaller airplanes, however, these solutions are often too large, heavy, or expensive, and commonly, only measurements from a Pitot-static tube are available.

[1, 2] employ unscented Kalman filter (UKF) and extended Kalman filter (EKF), respectively, to estimate the air- and ground-relative velocities from global navigation satellite system (GNSS) and airspeed measurements in addition to two vanes measuring AOA and SSA. [3] uses a multi-hole Pitot-static tube for the same purpose. For small unmanned aerial vehicles (sUAVs), these solutions are intrusive and expensive, respectively, and both require significant calibration.

A relatively inexpensive solution is the single hole Pitot tube. It only measures the airspeed, and therefore requires attitude changes over time to observe the wind velocity, assuming knowledge of the ground-relative velocity of the aircraft. From this, AOA, SSA, and airspeed can be calculated. This is done in [4], where a method using only kinematic relationships with the single-hole Pitot-tube is presented. There, a wind-velocity observer was proposed which required attitude and velocity signals in addition to airspeed measurements. Kalman filters (sKFs) for two different Pitot-static tube measurement models were proposed. In one, the Pitot-static tube was modeled to measure the forward-component of the air-relative velocity component in the body-fixed x-axis, and in the other, it was modeled to measure the airspeed. In the latter model, the Pitot-static tube was assumed mounted to a vane which ensures that it points in the direction of the relative velocity. This model is also appropriate for Pitot-static tube designs that are insensitive to small AOA and SSA, as shown in [5]. This is the Pitot-static tube model assumed in this paper.

If an accurate model of the aircraft is available, AOA, SSA, and airspeed can be estimated through a model-based approach. This approach is, however, prone to modeling errors. A combination of the model-based estimation and single-hole Pitot-static tube was presented in [6], where the wind velocity was estimated along with the coefficients of a generic fixed-wing aerodynamic lift model that only consists of a constant term and a linear term in AOA. Furthermore, the wind velocity was comparted into low- and high-frequency terms by frequency separation of the Dryden wind model. [7] achieves higher accuracy when solving the same problem with a moving-horizon estimator.

There also exists model-free approaches that do not use Pitot-tubes. In [8], a routine for estimating wind velocity without airspeed measurements and the use of an aircraft model is developed. By flying circle and helix patterns with constant throttle and pitch, assuming that this produces a constant airspeed, and inputing the ground velocity trajectory, the wind is solved for in an optimization problem.

The benefit of using a single-hole Pitot-static tube like the approach in [4] is that it is inexpensive relative to the multi-hole Pitot-tube and significantly less intrusive than using vanes, while requiring little pre-flight calibration since

*Postdoctoral researcher, bard.b.stovner@ntnu.no.
†Professor, tor.arne.johansen@ntnu.no.

the correction factor can be estimated online. Compared to the measurement-free approach of [8], it makes fewer assumptions and demands less maneuvers. It only measures the airspeed, and therefore requires attitude changes over time to observe the wind velocity, assuming knowledge of the ground-relative velocity of the aircraft. Since, when using a single-hole Pitot-static tube, the airplane must sweep over a range of attitudes in order for the system to be observable, this may have slower convergence than some of the mentioned alternatives. If one is interested chiefly in the steady component of the wind field, an assumption about constant or slowly varying wind velocity can be made. Then, fast convergence may not be as important.

In this paper, the Pitot-static tube measurements are used with ground velocity information to estimate the steady component of the wind field around a small fixed-wing UAV. A global exponential stability (GES) estimator based on the exogeonus Kalman filter (XKF) of [9] called the three-stage filter (3SF) is developed, and compared with a standard EKF and the KF of [4].

II. PRELIMINARIES AND MODELS

A. Notation

The Euclidean norm of a vector ν is denoted $\|\nu\|_2$. The transpose of the vector ν is denoted $\nu^\top$. A stochastic variable ϵ drawn from a Gaussian distribution with mean m and covariance S is denoted $\epsilon \sim \mathcal{N}(m, S)$. The Moore-Penrose pseudo-inverse is $A^\dagger = (A^\top A)^{-1} A^\top$.

The vector v^d_{ef} refers to the velocity of the coordinate frame $\{f\}$ relative to the coordinate frame $\{e\}$ decomposed in the coordinate frame $\{d\}$.

The global frame is in this paper the north-east-down (NED) frame, denoted $\{n\}$, while the body-fixed frame of the UAV is denoted $\{b\}$. The avarage motion of the air surrounding the UAV is denoted by the letter a, such that e.g. the air-relative velocity of the UAV decomposed in the body-fixed frame is denoted v^b_{ab}.

B. Measurement model

The Pitot-static tube measures the dynamic pressure Δp, i.e., the difference between the total pressure p_t at one point and the static pressure p_s at another. The dynamic pressure Δp is related to the airspeed through

$$\Delta p = p_t - p_s = \frac{1}{2}\rho \|v^b_{ab}\|_2^2$$

where ρ is the density of the surrounding air. Including noise and a correction factor γ to account for calibration errors, we model the dynamic pressure measurement y_p as

$$y_p = h_p(x,t) = \frac{\rho}{2}\gamma \|v^n_{nb} - v^n_{na}\|_2^2 + \epsilon_p \tag{1}$$

where $x = [v^n_{na}, \gamma]^\top$ is the state vector and $\epsilon_p \sim \mathcal{N}(0, R_p)$. The vectors v^n_{nb} and v^n_{na} are the ground velocity of the vehicle and the wind velocity, respectively.

C. Dynamic model

The state is assumed constant of slowly-varying and thus modeled as a random walk process

$$\dot{v}^n_{na} = \epsilon_a \tag{2a}$$

$$\dot{\gamma} = \epsilon_\gamma \tag{2b}$$

where $\epsilon_a \sim \mathcal{N}(0, Q_a)$ and $\epsilon_\gamma \sim \mathcal{N}(0, Q_\gamma)$.

III. Three-Stage Filter

In this section, the three-stage filter is developed. It is based on the XKF of [9] and the double KF of [10], and consists of an auxiliary estimator that is constructed in two stages and has the desired stability properties. The first stage is an algebraic manipulation of the non-linear measurement equation (1) that yields a linear measurement model. The second stage is a KF implemented on this linear model. Subsequently, in the third stage, the non-linear model (1) is

linearized about the estimate from the second stage, and a KF is implemented on the linearized model. This linearized KF now assumes the stability properties of the second stage estimator, which is GES in the case of a KF implemented on a linear model.

A. First Stage: Algebraic Solution

For simplicity of presentation, we define $x_1 = v_{na}^n$, $x_2 = 1/\gamma$, $a_k = v_{nb}^n(t_k)$, and $b_k = 2y_p(t_k)/\rho$, where the latter two are measured or estimated and an approximation of ρ is sufficient since γ is estimated. This allows us to rewrite (1) at $t = t_k$ as

$$b_k x_2 = x_1^\top x_1 - 2a_k^\top x_1 + a_k^\top a_k + \xi_k \tag{3}$$

where $\xi_k = 2x_2\epsilon_{p,k}/\rho$ the resulting noise term. Collect L inputs and stack into vector form like

$$0_{L\times 1} = \begin{bmatrix} x_1^\top x_1 - 2a_1^\top x_1 + a_1^\top a_1 - b_1 x_2 + \xi_1 \\ \vdots \\ x_1^\top x_1 - 2a_L^\top x_1 + a_L^\top a_L - b_L x_2 + \xi_L \end{bmatrix} = lr - Cx + d + e \tag{4}$$

where $r = x^\top M x$ and

$$l = \begin{bmatrix} 1 \\ \vdots \\ 1 \end{bmatrix} \in \mathbb{R}^L, \quad M = \begin{bmatrix} I_3 & 0_{3\times 1} \\ 0_{1\times 3} & 0 \end{bmatrix}, \quad C = \begin{bmatrix} 2a_1^\top & b_1 \\ \vdots & \\ 2a_L^\top & b_L \end{bmatrix}, \quad d = \begin{bmatrix} a_1^\top a_1 \\ \vdots \\ a_L^\top a_L \end{bmatrix}, \quad e = \begin{bmatrix} \xi_1 \\ \vdots \\ \xi_L \end{bmatrix}$$

Now, we solve for x in (4)

$$\begin{aligned} Cx =& lr + d + e \\ x =& C^\dagger l r + C^\dagger d + C^\dagger e = cr + z + C^\dagger e \end{aligned} \tag{5}$$

where $c = C^\dagger l$ and $z = C^\dagger d$. This requires that the matrix C is pseudo-invertible, i.e. that C has rank 4, see Assumption 1. By inserting this into the expression for r, we get

$$\begin{aligned} 0 =& (cr + z + C^\dagger e)^\top M (cr + z + C^\dagger e) - r \\ =& c^\top M c r^2 + (2z^\top M c - 1) r + z^\top z + e^\top C^{\dagger\top} M C^\dagger e \end{aligned}$$

In the above expansion, the cross term $2(cr+z)^\top M C^\dagger e$ is neglected since it is zero mean. The term $e^\top C^{\dagger\top} M C^\dagger e$ is however not zero mean, which we account for by replacing it with its expectation $E(e^\top C^{\dagger\top} M C^\dagger e) = L(2x_2/\rho)^2 R_p \text{trace}(C^{\dagger\top} M C^\dagger)$. Since in practice x_2 will be close to 1, we insert that here. The second order expression

$$0 = q_1 r^2 + q_2 r + q_3 \tag{6}$$

has the two solution for r

$$r_1, r_2 = \frac{-q_2 \pm \sqrt{q_2^2 - 4q_1 q_3}}{2q_1} \tag{7}$$

where $q_1 = c^\top M c$, $q_2 = 2z^\top M c - 1$, and $q_3 = z_3^\top z_3 + L(2/\rho)^2 R_p \text{trace}(C^{\dagger\top} M C^\dagger)$. We denote r_1 the correct solution and assume that the ambiguity can be resolved, see Assumption 2.

Now, a linear measurement function is acquired as

$$y_l = l r_1 + d = Cx - e \tag{8}$$

where $e \sim \mathcal{N}(0, R_l)$. We see that $R_l = E(ee^\top) = (2x_2/\rho)^2 R_p$, where we may insert 1 as the best a priori esimate for x_2.

Assumption 1 (Full rank of C) *It is in the derivation of the linear time-varying (LTV) measurement equation* (8) *assumed that C har rank 4. This is a persistency of exitation (PE) requirement that is met when the collection of $L \geq 4$ measurements are sufficiently rich in variation. The degree of exitation in the collection limits the esitmation accuracy possible with this model.*

Assumption 2 (Resolving the ambiguity in (6)**)** *It is assumed that the ambiguity in* (6) *can be resolved. In order to do this, one can calculate the possible solutions $x_1 = cr_1 + z$ and $x_2 = cr_2 + z$ of* (5) *and e.g. choose the solution that is closeset to the current state estimate or choose the solution with correction factor value closest to 1. The latter is done here.*

B. Second Stage: LTV KF

The second stage is an LTV KF based on the linear measurement model (8) constructed in the first stage. We denote its estimate $\bar{x} = [\bar{x}_1^\top, \bar{x}_2]^\top$ which is updated by

$$\dot{\bar{x}} = \bar{K}(y_l - C\bar{x}) \tag{9}$$

where $\bar{K}$ is the Kalman gain matrix of the stage 2 KF, found as the solution of the Riccati equation with covariance matrix $\bar{P}(t)$, process noise covariance matrix $Q = diag(Q_a, Q_\gamma)$ and measurement noise variance R_l.

C. Third Stage: Linearized KF

The third stage is a linearized KF about the estimate from the second stage KF. The state esimate for the third stage is $\hat{x} = [\hat{x}_{na}^n, \hat{\gamma}]^\top$.

Now, we find the vector used as linearization point in the third stage, $\breve{x}$, from the second stage exogenous state vector $\bar{x}$, by

$$\breve{x} = \begin{bmatrix} \breve{x}_1 \\ \breve{x}_2 \end{bmatrix} = \begin{bmatrix} \bar{x}_1 \\ 1/\bar{x}_2 \end{bmatrix} \tag{10}$$

so we can use the measurement model (1). This can be linearized about $\breve{x}$

$$h_p(x,t) = h_p(\breve{x},t) + H_p(\breve{x},t)(x - \breve{x},t) + \varphi(x - \breve{x},t) \tag{11}$$

where $\varphi(x - \breve{x},t)$ contain the higher order terms of linearization and $\varphi(0,t) = 0$. The measurement matrix if found as

$$H_p(\breve{x},t) = \begin{bmatrix} H_{pv}(\breve{x},t) & H_{p\gamma}(\breve{x},t) \end{bmatrix} \tag{12}$$

$$H_{pv}(\breve{x},t) = -\rho\breve{x}_2(v_{nb}^n(t) - \breve{x}_1)^\top \tag{13}$$

$$H_{p\gamma}(\breve{x},t) = \frac{\rho}{2}\|v_{nb}^n(t) - \breve{x}_1\|_2^2 \tag{14}$$

Now, the estimator is defined by

$$\dot{\hat{x}} = \hat{K}(y_p - h_p(\breve{x},t) - H_p(\breve{x},t)(\hat{x} - \breve{x})) \tag{15}$$

where the Kalman gain matrix $\hat{K}$ is found as the solution of the Riccati equation with covariance matrix $P_{s3}(t)$, process noise covariance matrix $Q = diag(Q_a, Q_\gamma)$ and measurement variance R_p.

D. Stability analysis

Since $\dot{x} = 0$ in the nominal case, we get that the estimation error $\tilde{x} \triangleq x - \hat{x}$ has the nominal dynamics

$$\dot{\tilde{x}} = -\dot{\hat{x}} = \hat{K}(H_p(\breve{x},t)(x - \hat{x}) + \varphi(x - \breve{x},t)) \tag{16}$$

It follows from [9] that the equilibrium point $\tilde{x}$ of the error dynamics (16) is GES if the system is uniformly completely observable (UCO). This is ensured over time under Assumption 1 and 2.

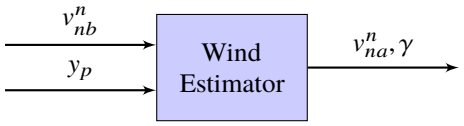

Fig. 1 The simple structure of the wind estimators.

IV. Simulations and Experiments

The filters that are tested with data from simulations and experiments are

- EKF: A classic EKF implementation using the dynamic model (2) and the measurement model (1)
- KF[4]: The KF estimator presented in [4]
- 3SF2: The second stage estimator of section III.B
- 3SF3: The third stage estimator of section III.C

Figure 1 shows the inputs and outputs of the 3SF developed in this paper and of the EKF used as benchmark. The velocity over ground might acquired from GNSS velocity measurements or other sensors or state esitamators. In the simulations and experiments in this paper, a state estimator is used which takes inertial measurement unit (IMU) and GNSS measurements and estimates the position, velocity, and attitude of the vehicle along with accelerometer and angular rate sensor (ARS) bias. Notice that the estimator from [4] additionally requires the attitude of the UAV.

Simulation study

A simulation study was conducted in order to compare the performance of the estimators in an ideal case with a known ground truth reference. The simulated scenario was a flight pattern rich in variation both in the horizontal plane and vertical direction. The estimators were run on the same simulated flight data 300 times with different measurement noise, wind field, and correction factor in each of the simulations. Mean absolute error (MAE) values computed from the results are presented in order to analyze both transient and stationary performances.

The wind velocity vector was for each simulation drawn from an unbiased Gaussian distribution with standard deviation of $3m/s$ for the horizontal directions and $0.3m/s$ for the vertical direction. The true Pitot-tube correction factor was drawn from a Gaussian process of mean 1 and standard deviation of 0.15. This ensured a wide range of winds and corrections factors in the simulated scenarios.

The noise variance of the dynamic pressure measurement was $R_p = 10^2$ (recall that the dynamic pressure measurement is the squared norm of the relative velocity). This value was also used in the tuning of the EKF, 3SF2, and 3SF3. Since the KF of [4] relies on airspeed measurements, the dynamic pressure measurements from the Pitot-tube were converted to airspeed by the first order power series approximation of the square root

$$\begin{aligned} y_{airspeed} =& \sqrt{\|v^b_{ab}\|^2 + \epsilon_p} = \|v^b_{ab}\| \sqrt{1 + \frac{\epsilon_p}{\|v^b_{ab}\|^2}} \\ \approx& \|v^b_{ab}\| (1 + \frac{1}{2} \frac{\epsilon_p}{\|v^b_{ab}\|^2}) = \|v^b_{ab}\| + \frac{\epsilon_p}{2\|v^b_{ab}\|} \end{aligned}$$

With a typical airspeed of $20m/s$, this yields an $R_{airspeed} = (\frac{10}{2 \cdot 20})^2 = .25^2$, which was used in the tuning of KF[4]. Since the algebraic manipulation in section III.A greatly amplifies the effect of the noise in (9), the measurement noise covariance of 3SF2 is chosen as $R_{s1} = 5$.

The process noise covariance matrix were set to $Q = diag(Q_a, Q_\gamma) = diag(10^{-5}, 10^{-5}, 10^{-5}, 10^{-6})$. The initial estimates of all estimators were $0m/s$ for all wind components and 1 for the Pitot-tube correction factor. The measurement frequency of the Pitot-tube measurements was 10Hz, with which state estimates were available also. The number of measurements gathered for the construction of the linear measurement model (4) is $L = 300$, which with a measurement rate of 10Hz means that the estimates of 3SF2 are updated every 30 seconds. If C is ill-conditioned, update of 3SF2 can be postponed until the vehicle's trajectory is sufficiently excited.

Figure 2 shows the wind velocity and correction factor estimate absolute errors averaged over the 300 simulations of 600 seconds each. The first 300 seconds are shown to display the transient behaviors of the estimators. From it, it can be seen that the transient behaviors are similar for all filters.

In order to study the robustness w.r.t. suboptimal tuning, the process noise covariance matrices were multiplied by a constant tuning factor κ while the measurement noise covariance matrices were divided my κ. Values of κ of 10 and 40

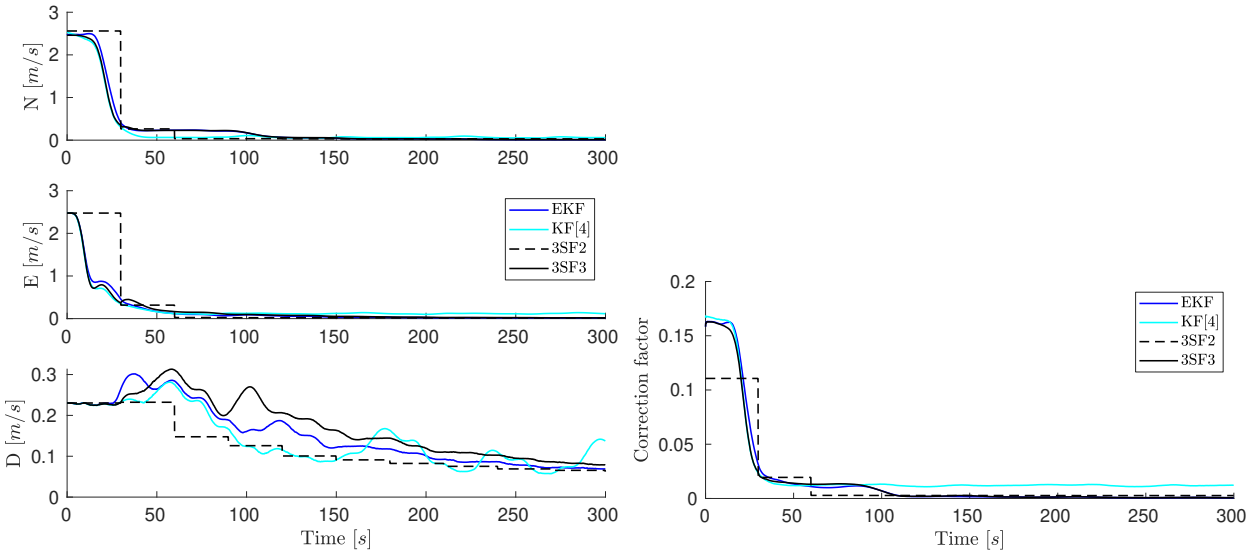

(a) Wind velocity error **(b) Correction factor error**

Fig. 2 Average error plots showing the transient performances of the filters with nominal tuning $\kappa = 1$.

were tested, which increased the process uncertainty and confidence on the measurements. Since KF[4] uses airspeed measurements, its noise covariance matrix was divided by $\sqrt{\kappa}$ instead. Figure 3 shows the absolute estimation errors averaged over the 300 simulations. It shows the increased robustness to suboptimal tuning achieved in the 3SF with respect to the EKF and KF[4].

Table 1 shows the MAE of the estimators after 300 seconds in order to compare steady state performances for $\kappa = 1$, $\kappa = 10$, and $\kappa = 40$. It shows that the suggested estimator 3SF3 performes near identically as the EKF in steady state when they are tuned well $\kappa = 1$, which is expected since they are both linearized KFs. In this casee, the table also shows that 3SF3 is a significant improvement over 3SF2. When $\kappa = 10$, KF[4] becomes significantly impacted by the suboptimal tuning, whereas the same happens for the EKF at $\kappa = 40$. The 3SF3 is also impacted by it, but much less than the EKF and KF[4]. This is owed to the robustness with respect to suboptimal tuning of the 3SF2, whose steady state performance is barely deteriorated with increasing κ.

Experimental study

The estimators are also tested with experimental data and compared. The estimates are compared with the estimates of the on-board Pixhawk autopilot and a least-squares estimate computed from the dataset as a whole ("Opt." in the Figure 4 and 5). The latter is the closest to a ground truth reference achievable from the flight data. It relies on the same data as all esimators, so it is sensitive to sensor errors and inaccuracies in the same way as the estimators.

All estimators were tuned identically to the extent that it was possible. The initial covariance matrix was $P_0 = diag(10^{-3}, 10^{-3}, 10^{-5}, 10^{-7})$, the process covariance matrix $Q = diag(Q_a, Q_\gamma) = diag(10^{-4}, 10^{-4}, 10^{-4}, 10^{-6})$, and the measurement variances $R_p = 15^2$ and $R_{airspeed} = 0.5^2$. In the experimental study, the number of measurements collected were $L = 1000$, which with a measurement rate of 10Hz meant that 3SF2 was updated every 100 seconds.

In Figure 4a–4b, the wind velocity and correction factor estimates from the experiments are seen. We see from the figure a similar steady state performance of all estimators. The estimator on the on-board computer "Pixhawk" did not estimate the wind in the vertical direction, and therefore it is constantly zero. The estimates of the vertical wind velocity eventually approaches the value found by the optimalization. The vertical component is less observable than the horizontal components since the airplane naturally has much greater accelerations in the longitudinal direction than the vertical. Therefore, the vertical wind velocity estimate should not be trusted too much.

The weights on the process covariance matrix are increased to $Q = diag(1e-1, 1e-1, 1e-1, 1e-3)$ in order to compare the sensitivity of the estimators. The result is, as shown in Figure 5, diverging behavior of the EKF and significantly more noisy behavior of KF[4] while the 3SF stays reasonably within bounds. Since KF[4] is the only estimator that relies on attitude information, the increased noise sensitivity under suboptimal tuning might also be

Table 1 MAEs of estimators of the steady state performance of the filters from 300-600 seconds. Notice that the values are multiplied by a factor of 100 for readability.

$\kappa = 1$	EKF	KF[4]	3SF2	3SF3
North$[cm/s]$	1.03	6.68	3.03	1.05
East$[cm/s]$	1.23	11.92	1.60	1.29
Down$[cm/s]$	5.14	8.13	4.92	5.60
$\gamma[\cdot 100]$	0.07	1.21	0.27	0.07
$\kappa = 10$	EKF	KF[4]	3SF2	3SF3
North$[cm/s]$	2.40	18.56	2.97	2.36
East$[cm/s]$	2.58	19.06	1.72	2.54
Down$[cm/s]$	8.93	13.21	3.92	8.89
$\gamma[\cdot 100]$	0.22	2.02	0.26	0.21
$\kappa = 40$	EKF	KF[4]	3SF2	3SF3
North$[cm/s]$	29.31	109.63	3.98	4.13
East$[cm/s]$	29.24	101.61	2.75	4.23
Down$[cm/s]$	47.72	44.01	6.80	12.80
$\gamma[\cdot 100]$	2.36	8.01	0.20	0.43

caused by noisy attitude estimates from the Attitude and heading reference system (AHRS). However, since KF[4] also suffered similarly from suboptimal tuning in the simulations, this cannot fully explain the deteriorated performance under suboptimal tuning. Although one might not tune the esimators so liberally in practice, it still displays the improved stability and robustness with respect to tuning and noise of the 3SF.

V. Conclusion

In this paper, a three-stage filter estimating the steady velocity of a wind field surrounding an unmanned aerial vehicle was developed. The estimator stability was analyzed and shown to be globally exponentially stable. In both simulations and experiments, the filter was shown to have similar steady state performance as a standard EKF implementation. Furthermore, it was shown that with s uboptimal tuning, the EKF diverged and failed to recover, while the proposed estimator still converged.

ACKNOWLEDGMENT

This work was supported by the Norwegian Research Council (grants no. 261791 and 223254).

References

[1] Rhudy, M. B., Larrabee, T., Chao, H., Gu, Y., and Napolitano, M., "UAV Attitude, Heading, and Wind Estimation Using GPS/INS and an Air Data System," *AIAA Guidance, Navigation, and Control (GNC) Conference*, 2013.

[2] Brossard, M., Condomines, J.-P., and Bonnabel, S., "Tightly Coupled Navigation and Wind Estimation for Mini UAVs," *AIAA GNC 2018, AIAA Guidance, Navigation, and Control Conference*, 2018.

[3] van den Kroonenberg, A., Martin, T., Buschmann, M., Bange, J., and Vörsmann, P., "Measuring the Wind Vector Using the Autonomous Mini Aerial Vehicle M2AV," *Journal of Atmospheric and Oceanic Technology*, Vol. 25, No. 11, 2008, pp. 1969–1982.

[4] Johansen, T. A., Cristofaro, A., Sørensen, K., Hansen, J. M., and Fossen, T. I., "On Estimation of Wind Velocity, Angle-of-Attack and Sideslip Angle of Small UAVs Using Standard Sensors," *International Conference on Unmanned Aircraft Systems (ICUAS)*, 2015, pp. 510–519.

[5] Gracey, W., "Measurement of Aircraft Speed and Altitude," *NASA report*, 1980.

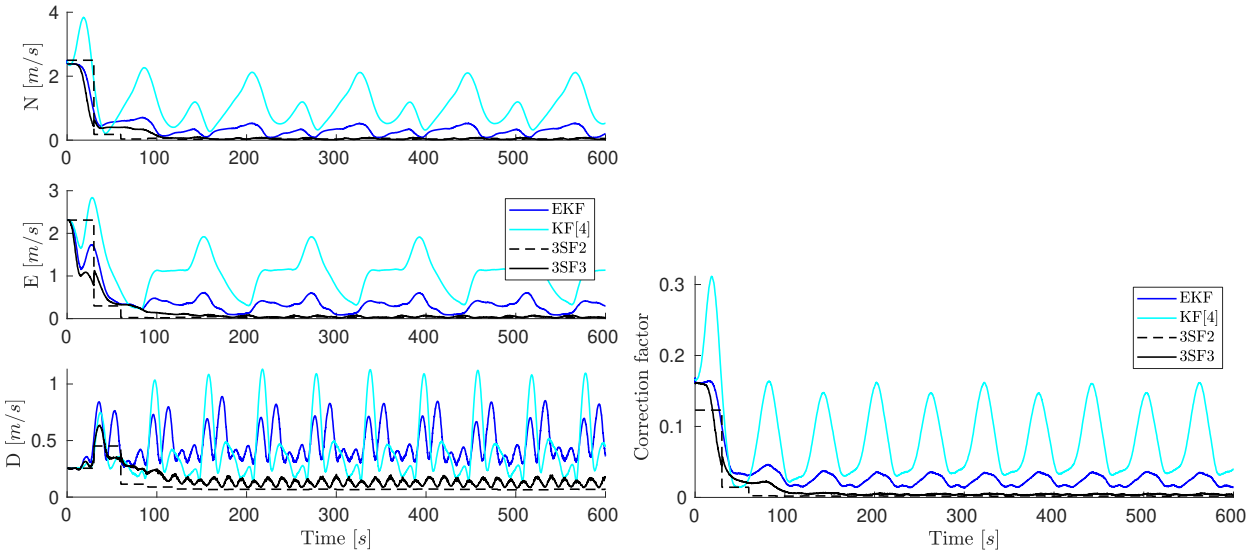

(a) Wind velocity error **(b) Correction factor error**

Fig. 3 Average error plots showing the performances of the filters under suboptimal tuning with tuning factor $\kappa = 40$.

[6] Wenz, A., Johansen, T. A., and Cristofaro, A., "Combining Model-Free and Model-Based Angle of Attack Estimation for Small Fixed-Wing UAVs Using a Standard Sensor Suite," *International Conference on Unmanned Aircraft Systems (ICUAS)*, 2016, pp. 624–632.

[7] Wenz, A., and Johansen, T. A., "Moving Horizon Estimation of Air Data Parameters for UAVs," *IEEE Transactions on Aerospace and Electronic Systems*, 2019.

[8] Mayer, S., Hattenberger, G., Brisset, P., Jonassen, M. O., and Reuder, J., "A 'No-Flow-Sensor' Wind Estimation Algorithm for Unmanned Aerial Systems," *International Journal of Micro Air Vehicles*, Vol. 4, No. 1, 2012, pp. 15–29.

[9] Johansen, T. A., and Fossen, T. I., "The eXogenous Kalman Filter (XKF)," *International Journal of Control*, Vol. 90, No. 2, 2017, pp. 161–167.

[10] Johansen, T. A., and Fossen, T. I., "Nonlinear Filtering with Exogenous Kalman Filter and Double Kalman Filter," *2016 European Control Conference (ECC)*, 2016, pp. 1722–1727.

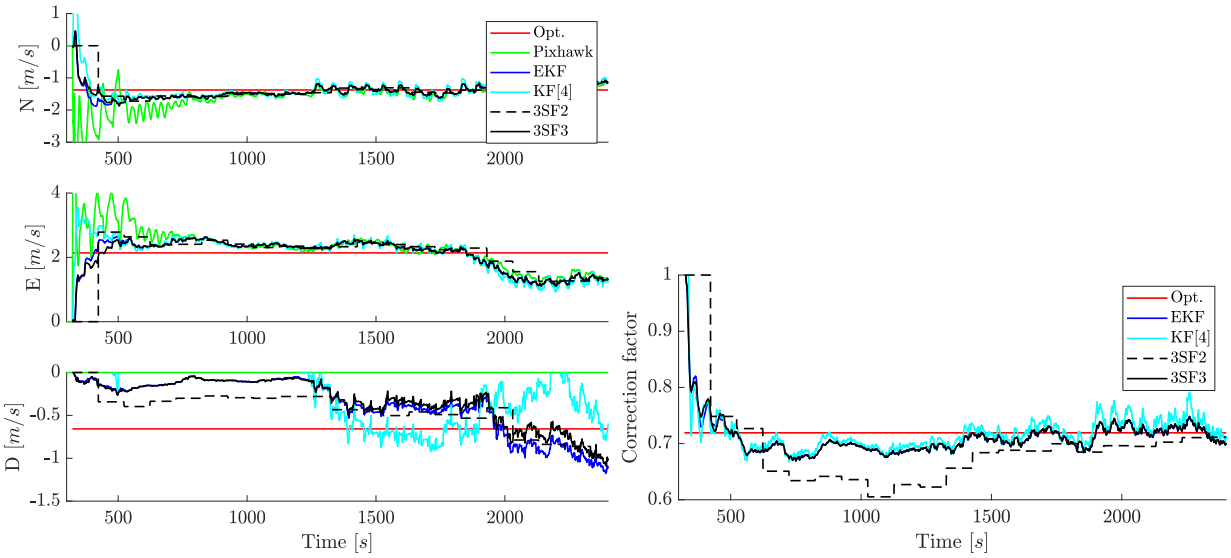

(a) Wind velocity estimates. **(b) Correction factor γ.**

Fig. 4 Comparison of estimates from experiments. "Opt." is the least squares optimal solution over the whole data set.

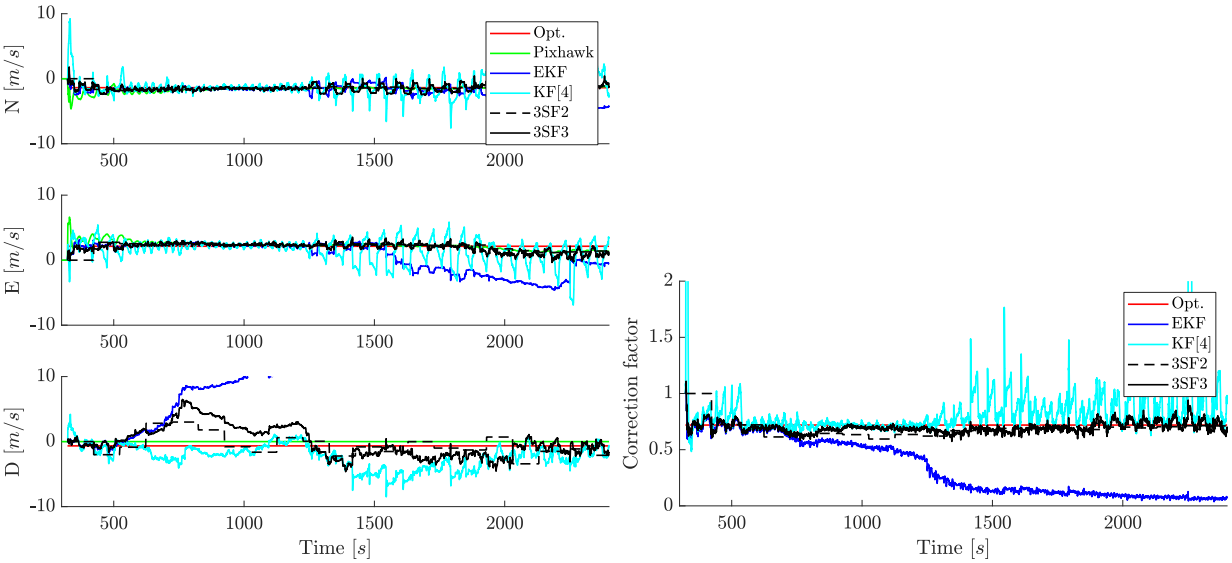

(a) Wind velocity estimates **(b) Correction factor γ.**

Fig. 5 This figure shows the results from the same dataset at Figure 4, but with greater weights in the process covariance matrix.